GEN Biotechnology
Volume 3, Number 6, 2024

DOI: 10.1089/genbio.2024.0043

GEN Biotechnology

RESEARCH ARTICLE

Real-Time Monitoring in Biomanufacturing with Graphene Field-Effect Transistor Sensors: Detection of pH, Glucose, and Antibodies

Deependra K. Ban,[1,†] Reza Hajian,[2,3,†] Matthew Chan,[2,†] Shiva Abdolrahimi,[4] Francie Barron,[5] Saurav Datta,[4] and Kiana Aran[1,5,6,*]

Abstract

In high-efficiency smart biomanufacturing, continuous monitoring of products, byproducts, and reagents is crucial for optimizing production processes, improving yield, and ensuring product quality. This monitoring maintains optimal conditions, reduces waste, and enables swift corrective actions, minimizing the risk of producing out-of-specification products. With advancements in cell-free biomanufacturing, the importance of in-line sensing technologies has increased, as they provide real-time tracking of biochemical processes, allowing immediate adjustments to keep manufacturing efficient and consistent. In this study, we successfully developed a graphene field-effect transistor (gFET) sensor to monitor key parameters such as glucose, pH, and immunoglobulin G antibody levels in cell culture media from a CHO cells bioreactor. The gFET sensor accurately detected pH levels between 6.8 and 8.2, glucose concentrations from 5 to 30 mM, and antibody levels ranging from 25 to 100 μg/mL, highlighting the potential of graphene sensors for inline sensing in advanced biomanufacturing.

Inline monitoring in bioprocessing plays a crucial role in optimizing the production process to ensure high product quality. By continuously tracking various critical parameters such as pH, temperature, nutrient levels, and metabolic outputs, inline monitoring systems allow for real-time adjustments and control. This immediate feedback loop helps in maintaining the bioreactor environment within optimal limits, thereby improving yield and reducing the risk of process deviations that could lead to product variability or batch failure. Furthermore, inline monitoring is crucial for implementing efficient process frameworks, which aim to design, analyze, and control the manufacturing process to guarantee product quality through timely measurements. This not only ensures compliance with regulatory standards but also enhances process efficiency by reducing downtime and waste to achieve consistent bioprocess performance.[1,2]

Several critical parameters such as pH, dissolved oxygen, temperature, and nutrient concentrations such as glucose, metabolite levels, cell density and viability, and product concentration must be closely monitored to ensure optimal conditions for cell growth and product formation. While the temperature and contaminants can be controlled through quality temperature modules and sterile conditions, glucose levels and pH require continuous monitoring to ensure optimal cellular growth and productivity.[3] Maintaining appropriate concentrations of nutrients, including glucose, is crucial to promote rapid growth and improved productivity, while excessive or insufficient amounts can hinder growth and product formation.[4] Even minor changes in pH of 0.1 units can affect cell growth rate. pH alteration due to metabolite consumption and high concentrations of lactate can lead to decreased cell growth and premature cell death.[5–7] To maintain the pH of the cell culture media sodium bicarbonate, base addition, and CO_2 sparging are typically used. Biomolecules production such as antibodies can only be monitored by techniques such as enzyme-linked immunosorbent assay, protein A/G high-performance liquid chromatography-ultraviolet, surface plasmon resonance, biolayer interferometry (BLI), and capillary electrophoresis-mass spectrometry.[8] All of

[1]Shu Chien-Gene Lay Department of Bioengineering, Jacobs School of Engineering Department of Bioengineering, University of California, San Diego, California, USA; [2]School of Applied Biosciences, Keck Graduate Institute, Claremont, California, USA; [3]Rapid Diagnostics Division, Abbott Laboratories, Pomona, California, USA; [4]Amgen Bioprocessing Center, Keck Graduate Institute, Claremont, California, USA; [5]Cardea Bio Inc., San Diego, California, USA; and [6]Department of Medicine, Division of Geriatrics, Gerontology & Palliative Care, School of Medicine, University of California, San Diego, California, USA.
[†]Equal first authors.
[2]Past affiliation of Reza Hajian.

*Address correspondence to: Kiana Aran, PhD, Shu Chien-Gene Lay Department of Bioengineering, Jacobs School of Engineering Department of Bioengineering, University of California, San Diego, CA 92093, USA, E-mail: karan@ucsd.edu

these measurement techniques involve taking samples from the bioreactor for offline time-delayed measurements, using multiple different instrumentations.[9] To overcome this, inline multianalyte analysis systems are crucial for effective monitoring of biomolecules in bioreactors. Graphene biosensors offer a promising technology for monitoring critical parameters in bioprocessing due to their high sensitivity, low sample requirement, multianalyte detection capabilities, and electrical output. These attributes make them ideal for real-time monitoring of a wide range of bioprocessing parameters. The unique properties of graphene allow for the rapid detection of changes in bioprocessing parameters, enabling immediate adjustments to the bioreactor environment.[10–13] In this report, we describe the development and testing of graphene biosensors designed for monitoring pH, glucose, and antibody levels (Figs. 1 and 2).

Results

To achieve optimal antibody yield in CHO cell cultures, it is essential to continuously monitor critical parameters such as pH, glucose levels, and antibody concentrations. In this study, we have designed and fabricated a single-platform graphene field-effect transistor (gFET) sensor system. This system was specifically functionalized with selective reporter or capture molecules tailored for monitoring pH, glucose, and immunoglobulin G (IgG) levels within both buffer solutions and cell culture media. The gFET sensors we developed underwent rigorous characterization, following protocols detailed previously.[11,14–16]

Glucose Sensing

The enzymatic reaction of glucose oxidase (GOX) with its substrate, D-glucose, results in the production of gluconic acid and hydrogen peroxide (H_2O_2).[17] To evaluate the gFET sensor's ability for real-time monitoring of H_2O_2, we conducted an initial experiment where H_2O_2 concentrations were incrementally increased in 1X phosphate-buffered saline (PBS), with 1X PBS alone serving as the control (Supplementary Fig. S1). The resulting Dirac voltage shifts, plotted to generate a calibration curve for H_2O_2 (Supplementary Fig. S1), showed a linear response slope of −1.65 mV/μM after a 5-min incubation and −1.68 mV/μM after a 10-min incubation. Additionally, the sensor's response to D-glucose alone, in the absence of GOX, was examined. The concentration-dependent Dirac shifts for the buffer and glucose showed overlapping responses for the 5-min measurements, with a minimal shift of −12 mV ± 0.3 mV at 30 mM glucose. A longer 10-min exposure to glucose resulted in a maximum Dirac shift of −30 ± 8.2 mV with respect to 1X PBS baseline (Supplementary Fig. S1). These experiments validate the gFET sensor's functionality in detecting biochemical changes and its potential application in biosensing platforms.

GOX functionalized gFETs (GOX-gFETs) were fabricated by immobilizing GOX to the surface of the gFET using 1-pyrenebutyric acid (PBA) as a linking agent. The immobilization process resulted in a significant alteration of the gFET's electronic properties, as demonstrated by a −70 ± 7.6 mV shift in the Dirac voltage post-immobilization, which is shown in Figure 3A. In contrast, the buffer alone exhibited an insignificant Dirac shift.

Following the immobilization, glucose detection assays were carried out using the GOX-gFETs previously tested for GOX conjugation (Fig. 3A). Figure 3B illustrates a nonlinear negative Dirac shift corresponding to increasing glucose concentrations, in contrast to the negligible changes observed with 1X PBS alone (Fig. 3B). Specifically, the introduction of glucose at the lowest concentration tested, 5 mM, led to a Dirac shift of −16 ± 3.4 mV, while the highest concentration, 30 mM, resulted in −67 ± 9.1 mV shift at pH 7.5. These shifts are attributed to the enzymatic activity of GOX when exposed to D-glucose.

Further monitoring of the effect of pH on GOX activity demonstrated a reduction in enzymatic efficiency at pH levels of 5 and 6, evidenced by Dirac shifts to −56.3 ± 8.1 mV and

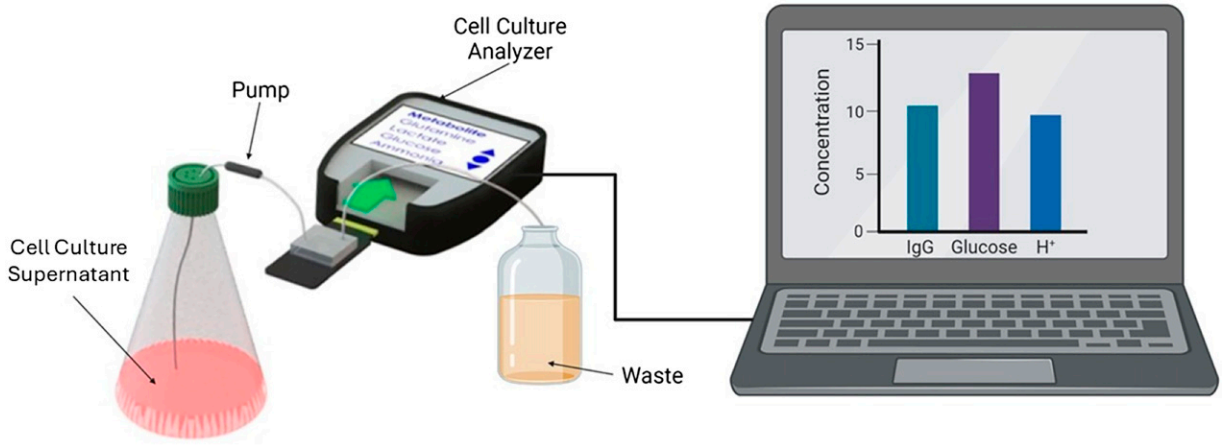

FIG. 1. gFET-based sensing of pH, glucose, and antibody in cell culture media.
gFET, graphene field-effect transistor.

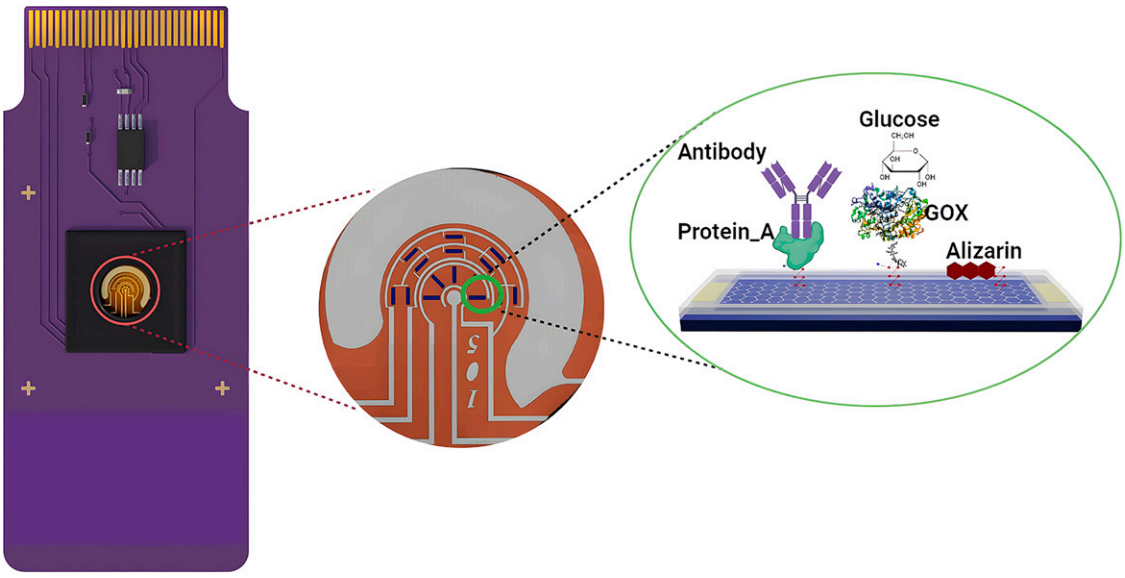

FIG. 2. The gFET sensor.

The zoomed-in section highlights the sensor design, focusing on a single graphene channel (green circle). The accompanying illustration shows the integration of different functional elements: Protein A for antibody detection, GOX for glucose detection, and Alizarin as a pH reporter on the gFET sensors (Created with BioRender.com). GOX, glucose oxidase.

−46.7 ± 8.5 mV, respectively. This reflects a sharp decrease in GOX activity to 16% and 31% at pH 5 and 6, respectively. In contrast, the 1X PBS background response was minimal at −4.9 ± 2.7 mV (Fig. 3B). This deviation from the concentration-dependent response observed at pH 7.5, as shown in Figure 3B, highlights the importance of calibrating GOX-based glucose detection according to pH to achieve accurate results. Additionally, specificity analysis of the GOX-functionalized sensor with D-glucose and L-glucose revealed distinct enzymatic activities. Specifically, a smaller Dirac shift of −18.4 ± 2.1 mV for 10 mM concentration of L-glucose was recorded (Fig. 3C), compared with a −47.38 ± 2.7 mV shift for the same concentration of D-glucose, indicating the sensor's ability to differentiate between the two glucose isomers.

We have further tested the GOX-gFET by administrating cell culture media and D-glucose-doped media (Fig. 3D). The results indicated that the complex components of the media induced a higher background signal, reaching up to −169 ± 2.3 mV. When transitioning from buffer to cell culture media, the introduction of varying concentrations (0–10 mM) of glucose-doped media samples resulted in Dirac voltage shifts, ranging from −158 ± 9.8 to −192.6 ± 5.4 mV for glucose levels between 0.1 and 10 mM, due to the GOX enzymatic reaction (Fig. 3D and Supplementary Fig. S2). Despite the change in media, the results were consistent with those obtained from commonly used systems such as the Roche CEDEX analyzer, showing a close correlation in sensor responses (Fig. 3E). Reusability tests of the GOX-gFET (chips, $n = 3$) also demonstrated mean Dirac shifts of 26.7 ± 0.9 mV up to four cycles with 5 mM of glucose (Supplementary Fig. S2).

pH Monitoring

For pH monitoring, we utilized alizarin, an aromatic pH reporter molecule (Supplementary Fig. S3), and compared various pH levels and media conditions. While unfunctionalized graphene can sense pH changes accurately in buffer solutions, its effectiveness diminishes in complex environments like cell culture media. To address this, three samples of 20 mM Tris-HCl were prepared at different pH levels (pH 6.8, pH 7.6, and pH 8.2) and applied to separate sensors. A Dirac response ranging from −31.9 ± 8.6 to −129.8 ± 7.4 was observed as the pH of the buffer increased from 6.8 to 8.2 (Fig. 4A). However, when 2.5% cell media was added, the Dirac shift decreased −40.2 ± 6.8 to −20.09 ± 10.8 mV for pH levels from 6.8 to 7.6 (Fig. 4B), indicating that the complex media components interfere with the sensor's response. The presence of cell media alone not only quenched the Dirac response as pH increased from 6.8 to 8.25 but also caused a nonlinear sensor response to pH changes (Fig. 3C). To address this, we introduced the pH-sensitive molecule alizarin and first verified the pH-dependent Dirac shift ranging from 30.3 ± 4.8 mV to −111.8 ± 11.4 mV for Tris-HCl buffer of pH levels 6.8–8.25 (Fig. 4C). Further testing with 2.5% cell culture media in a pH range of 7.02–8.2 revealed a negative Dirac shift of −16.4 ± 11.3 to −90.7 ± 3.35 mV, reflecting a pH-dependent change in stable protonation state of alizarin (Fig. 3D); therefore, enabling more accurate pH monitoring (Fig. 4C, D).

Antibody Detection

For monitoring antibody levels, first, we measure the Dirac response to the protein A conjugated gFET (Fig. 5A). After 30-min incubation, the association and dissociation signal of

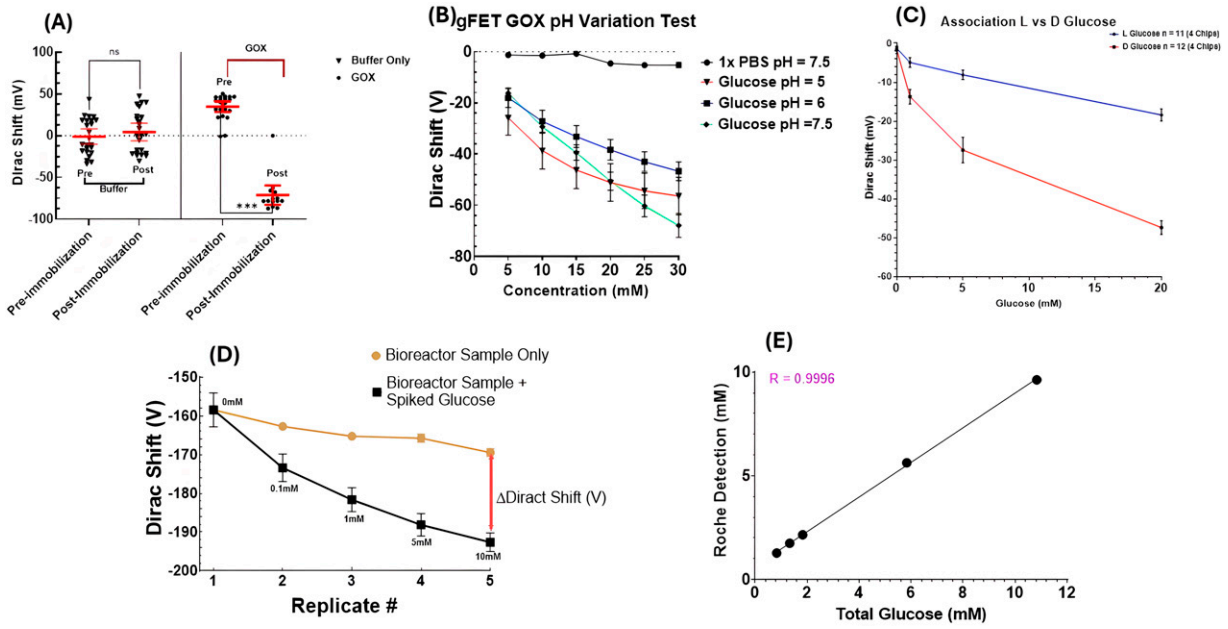

FIG. 3.

(A) gFET sensor response buffer control treated sensor showed overlapped Dirac sift, while GOX caused conjugation −70 ± 7.6 mV of Dirac shift.

(B) pH-dependent GOX activity analysis with 0–30 mM of D-glucose showed a Dirac shift of −25.8 ± 7.5 to −56.4 ± 8.1 mV for pH 5, −17.9 ± 8.8 to −46.7 ± 8.5 mV for pH 6, and −16.2 ± 3.4 mV to −67.8 ± 9.1 mV for pH 7.5.

(C) 20 mM of L-glucose and D-glucose exposure to GOX showed Dirac shift of −18.4 ± 2.1 mV and −47.38 ± 2.7 mV, respectively.

(D) Administration of cell culture media alone on the GOX-gFET induced a Dirac shift of −164.3 ± 4.1 mV, while the presence of GOX activity resulted in a shift of −158 ± 9.8 to −192.6 ± 5.4 mV for 0–10 mM D-glucose doped into the same media. All measurements presented here used n ≥ 9 transistor data to calculate mean ± standard deviation.

(E) Roche CEDEX, a confirmatory test for GOX activity showed a concentration-dependent linear response of 2–10 Roche detection (mM) for D-glucose (1–10 mM) doped cell culture media.

protein A were measured. The association of protein A resulted in a positive Dirac shift of 14 ± 2.4 mV, in contrast to the blank control (1X PBS), which exhibited a negative shift of −13.1 ± 1.8 mV (Fig. 5A). The dissociation signal for chips treated with protein A showed clustering around 29.4 ± 2.5 mV, whereas chips treated with the blank control (1X PBS) primarily clustered around 13.2 ± 1.1 mV (Supplementary Fig. S4).

Protein A immobilized chips were treated with samples of human IgG1 at sequentially increasing concentrations (Fig. 5). The concentration-dependent negative Dirac shift was observed for IgG1 compared with the control and reached saturation −13.8 ± 5 mV±) as the concentration increased from 50 to 100 μg/mL for the association signal (Supplementary Fig. S4) and −4.1 ± 0.81 to 8.1 ± 0.5 mV for the dissociation signal (Fig. 5B).

For specificity analysis, the Dirac response of protein A immobilized chips treated with 50 μg/mL human IgG1 was compared with those treated with 100 μg/mL Human IgG3. In Figure 4D, the association signal with serum IgG1 showed −11.7 ± 0.93 mV of Dirac shift while IgG3 showed −7.0 ± 1.5 mV. The difference in gFET sensor association response clearly showed a stronger association of IgG1 by protein A compared with IgG3 (Fig. 5D).

We have further monitored CHO cell filtrate containing IgG1 by doping 0, 0.1, and 0.5% v/v (Fig. 5C) in 1X PBS. The cell culture media (0.1%) without antibody causes Dirac shift below 5 mV, while 0.1% and 0.5% filtrate containing antibody Dirac response increase to −14.0 ± 0.45 mV and −15.9 ± 1.2 mV (Fig. 5C). We have further verified antibody level in our samples using Blitz, a BLI method, and using a protein A-based capture mechanism (Fig. 5E and Supplementary Fig. S4). The biolayer interferometer-based orthogonal methods showed the concentration-dependent response of the sensor both in the buffer as well as in cell culture filtrate containing IgG1 (Fig. 4E).

Discussion

In this study, we demonstrated the successful development and application of a gFET sensor for monitoring key parameters in cell culture media obtained from a CHO cells bioreactor, particularly focusing on glucose levels, pH, and IgG antibody levels.

Glucose serves as a crucial carbon source for IgG production, making it essential to maintain its optimal levels using inline detection tools. Although the sensor showed slight quenching

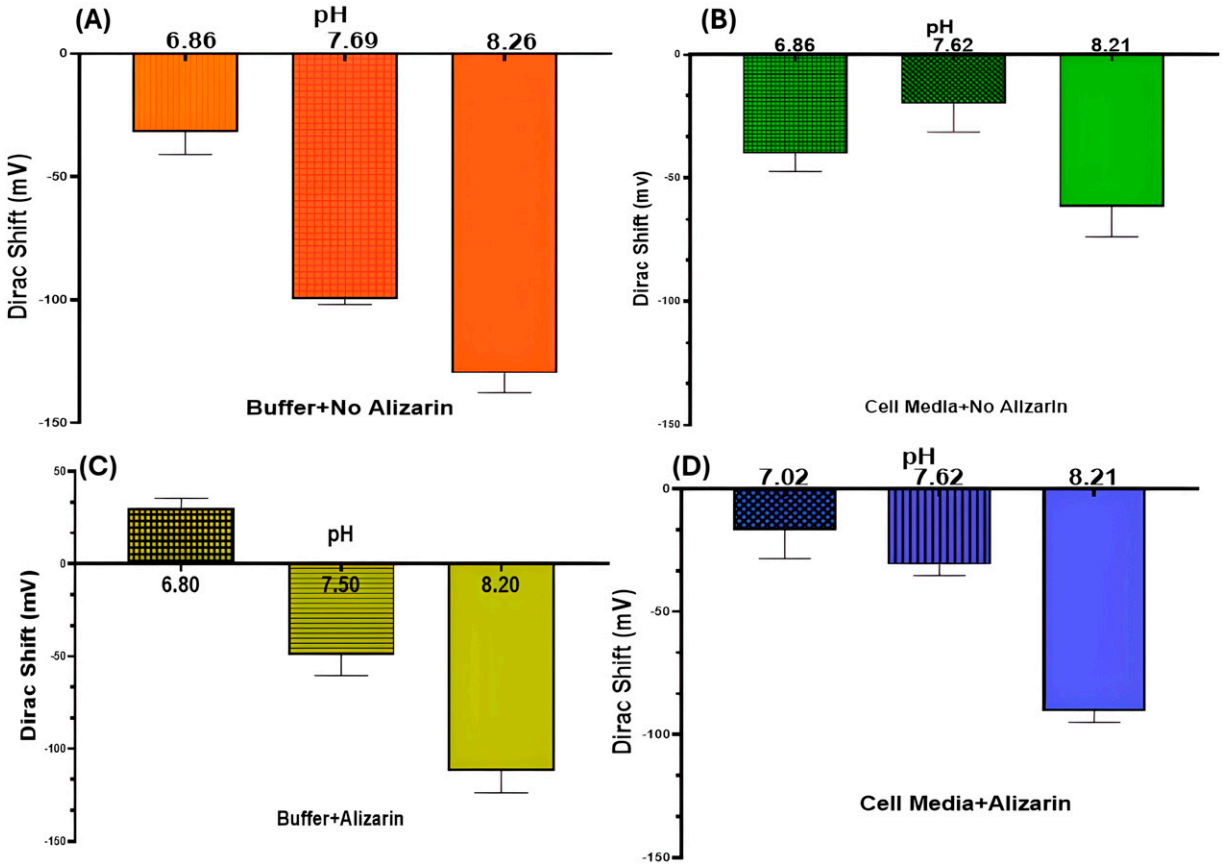

FIG. 4.

(A) gFET sensor was exposed to Tris-HCl buffer of pH 6.8, pH 7.6, and pH 8.2 induced Dirac shift of –31.9 ± 8.6, –99.6 ± 2.1, and –129.8 ± 7.4, respectively.

(B) 2.5% (v/v) DMEM media pH adjusted to 6.8, 7.6, and 8.2 using Tris-HCl buffer causes Dirac shift of –40.2 ± 6.8, –20.09 ± 10.8, and –61.6 ± 11.7 mV, respectively.

(C) Tris-HCl buffer of pH 6.8, pH 7.6, and pH 8.2 mixed with alizarin (25 μM) induced Dirac shift of 30.3 ± 4.8, –49.3 ± 10.5, and –111.8 ± 11.4 mV, respectively.

(D) 2.5% (v/v) DMEM media pH adjusted using Tris-HCl buffer with 25 μM alizarin dye showed Dirac shift of –16.4 ± 11.3 to –90.7 ± 3.35 mV for media with pH 7.02 to 8.21. The pH-dependent Dirac response and standard deviation were calculated using n ≥10 transistor data for each sample.

at lower pH levels (5 and 6) due to altered GOx enzymatic activity, it still effectively monitored the concentration-dependent Dirac shift, confirming its reliability as a glucose detection tool. The slight deviation in sensor response at lower pH (5 and 6) could be due to the intrinsic pH sensitivity of the gFET sensor combined with pH-dependent variations in GOx redox activity.[18–21] At lower pH values, the GOx redox mechanism is influenced by protonation changes, leading to different electron-transfer pathways. Specifically, below pH 6, GOx follows an ECEC mechanism (electron transfer followed by a chemical reaction), while above pH 6, an ECE mechanism (electron transfer, electron transfer, chemical reaction) predominates.[18–20] These shifts in redox activity and pH sensitivity of gFET can cause deviations in the sensor response, particularly at lower pH, resulting in the quenching effect observed. Despite these variations, the sensor maintained strong concentration-dependent behavior, confirming its potential for glucose detection and suggesting it could also be adapted to monitor insulin levels using specific antibodies or aptamers.[22] The sensor's multianalyte detection capability for simultaneous pH monitoring ensures accurate glucose measurement and calibration across varying conditions. This highlights the importance of calibrating the GOX-based sensor for accurate glucose measurement across different pH levels, ensuring that as culture conditions change, the sensor can provide accurate, normalized readings.

For pH sensing, the gFET sensor showed a linear response both with and without the addition of the alizarin reporter in

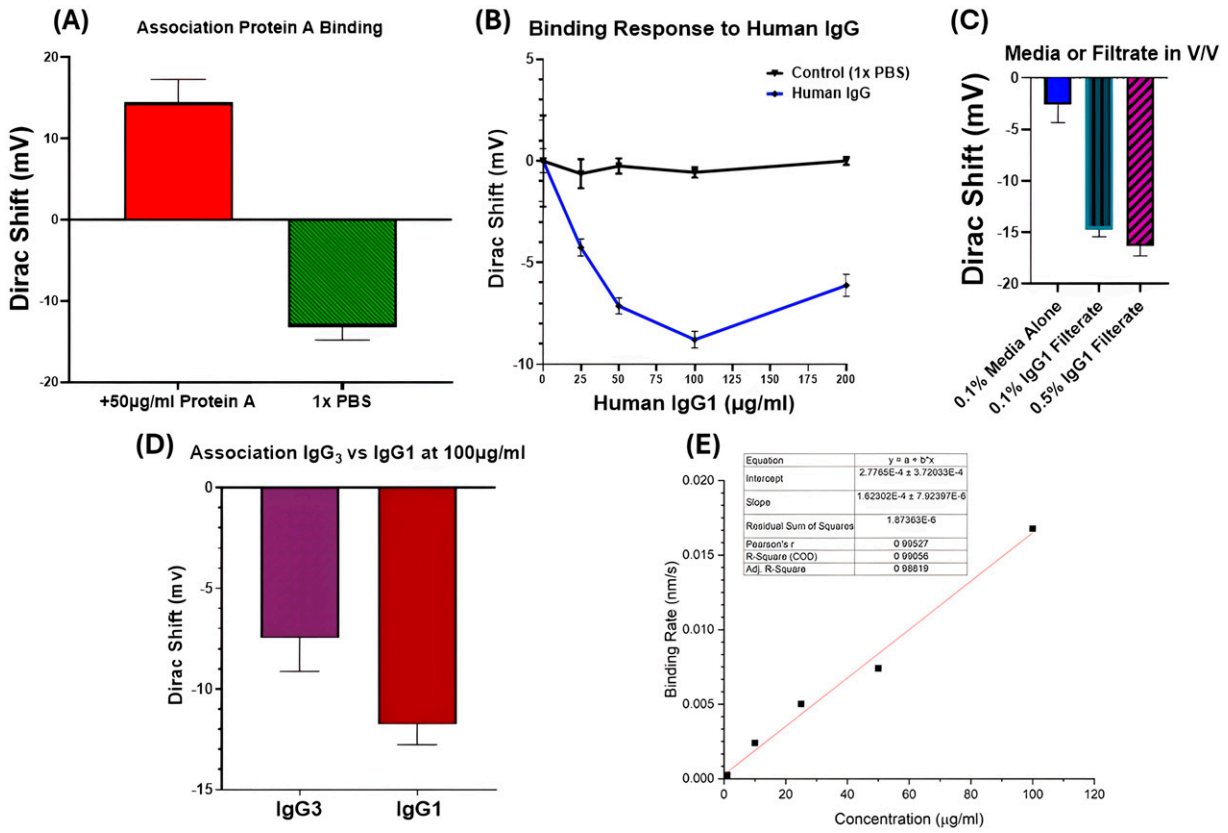

FIG. 5.

(A) Protein A conjugation induced Dirac shift of 14 ± 2.4 mV, while Buffer background causes negative −13.1 ± 1.8 mV.
(B) Concentration-dependent (0–100 µg/mL) IgG1 capture by protein A (50 µg/mL) functionalized chip induced concentration-dependent negative Dirac shift of −4.1 ± 0.81 to 8.1 ± 0.5 mV for 25–100 µg/mL and further increment of IgG1 to 200 µg/mL quenched the sensor response.
(C) Different amounts (0.1%, 0.5% v/v) of filtrate containing IgG1 showed Dirac shift of −14.4 ± 0.4 to −15.9 ± 1.2 mV. n ≥ 9, total transistor response used to calculate mean Dirac shift ± standard deviation.
(D) 100 µg/mL IgG3 and IgG1 were exposed to separate protein A functionalized chip (n = 3) and showed differential sensor response of −7.0 ± 1.5 mV and −11.7 ± 0.93 mV, respectively.
(E) IgG1 concentration binding with protein A was analyzed using BLITz, a BLI analysis (n = 3). BLI, biolayer interferometry.

buffer (Fig. 4A). However, the introduction of cell culture media to the gFET also quenched the pH signal, causing a nonlinear response and reducing the sensor's sensitivity at pH 7.5. This effect is likely due to the variable isoelectric points of different analytes in the media at various pH levels.[23] The inclusion of alizarin helped stabilize the response, likely due to its pH-dependent protonation state,[24] which provided a more consistent interaction with the graphene surface and resulted in a more linear response (Fig. 4C, D). Alizarin dye interaction causes positive Dirac potential shift due to an increase in hole current at pH 6.8 buffer, while above neutral pH (i.e., the buffer of pH 7.5 and 8.2), alizarin interaction with graphene increases negative charge carrier hence negative Dirac shift (Fig. 4C).

pH changes in DMEM cell culture media containing Alizarin interestingly showed a smaller Dirac shift for a pH change of 0.60 (from pH 7.02 to 7.62) compared with the larger Dirac shift with a pH change of 0.59 (from pH 7.62 to 8.21) attributed to the differential distribution of charged components in the media. This suggests that the net charge distribution in the medium and its interaction with both graphene and Alizarin, varies in a pH-dependent manner, leading to different sensor responses for nearly identical pH intervals (Fig. 4D). The more pronounced response between pH 7.62 and 8.21 reflects the greater change in charge distribution led to stronger interaction at more alkaline pH values.

The gFET sensor also demonstrated its capability for IgG1 detection, showing a concentration-dependent Dirac shift both in buffer and cell filtrate (Fig. 5). However, concentrations beyond 100 µg/mL led to a hook effect, where higher analyte concentrations caused a quenching of the sensor response—a common issue in various optical and sensing techniques, typically mitigated by analyte dilution.[25,26]

Lastly, our specificity analysis revealed a slight differentiation between IgG1 and IgG3, with a mean Dirac shift difference of about 2 mV (Fig. 5D). This suggests some degree of nonspecific adsorption of antibodies on the graphene surface. Future work will focus on optimizing passivation strategies, such as using PEG of varying lengths and polarities, to reduce nonspecific adsorption and improve sensor performance. Such strategies will also facilitate the development of an inline sensing module capable of handling higher analyte titers in CHO cell cultures, exceeding the currently reported highest concentration of 100 μg/mL.[13]

Conclusion

In high-efficiency smart biomanufacturing, continuous monitoring helps maintain optimal parameters, reduce waste, and enable quick corrective actions, minimizing the risk of out-of-specification products.[27] The integration of advancements in cell-free biomanufacturing has further emphasized the importance of in-line sensing technologies by facilitating immediate adjustments of biochemical processes and ensuring efficient and consistent.[28] As cell-free systems are not bound by the homeostatic requirements of living cells, they offer enhanced adaptability and precision in production, making in-line sensing a pivotal tool for achieving the full potential of smart biomanufacturing. This combination of advanced monitoring and in-line sensing not only supports the sustainable and cost-effective production of biomolecules but also ensures compliance with stringent regulatory standards, particularly in industries like biopharmaceuticals.[28]

The potential utilization of graphene sensors is significant in biomanufacturing processes, particularly as the industry moves toward more efficient, precise, and sustainable production methods. These sensors require less energy to operate, which aligns with the increasing demand for energy-efficient technologies in biomanufacturing. This energy efficiency is crucial in reducing the overall operational costs and environmental footprint of biomanufacturing facilities. One of the key advantages of graphene sensors is their exceptional sensitivity, enabling the detection of minute changes in biological and chemical environments. This sensitivity is vital for monitoring the complex and dynamic processes inherent in biomanufacturing, such as protein and antibody production. Furthermore, it ensures the activity of essential reagents, like enzymes, which can diminish over time or be adversely affected by byproducts generated during bioreactions. The ability to detect these changes in real-time allows for immediate adjustments to be made in the production process, ensuring consistent product quality and minimizing waste.

In conclusion, the integration of graphene sensors into biomanufacturing represents a significant step forward, combining energy efficiency with high sensitivity and stability. As the industry continues to evolve, the adoption of these advanced materials will be key to unlocking new possibilities in biosensing, ultimately leading to more effective and efficient biomanufacturing processes.

Materials and Methods

Materials

Tris-HCl at pH 7.5 and pH 8.5 (UltraPure™ 1 M, Invitrogen), and 1X PBS (Gibco™) from Thermo-fisher were utilized as buffers for the study. The pH indicator dye, alizarin (SKU:122777), was obtained from Sigma-Aldrich. Additional reagents such as H_2O_2, 1-PBA, and 1-pyrenebutyric acid *N*-hydroxyscuccinimide ester (PBASE), *N*,*N*-Dimethylformamide (DMF), 200% proof ethanol (EtOH), isopropyl alcohol (IPA), 1-Ethyl-3-(3-dimethylaminopropyl) carbodiimide (EDC), and 2-(*N*-morpholino)ethanesulfonic acid (MES) were also purchased from Sigma-Aldrich. For cell culture, DMEM media was used for CHO cells, and antibody filtrate was collected from Amgen Bioprocessing Center (Keck Graduate School, Claremont, USA). Protein A (P7155) and ex-cell advance CHO Fed-Batch Medium (14366C—1000 mL) were sourced from Sigma-Aldrich. Additionally, IgG1 (DDXCH01P-100) and IgG3 (DDXCH03P-100) were procured from Novus Biologicals.

Methods

gFET fabrication

Fabrication of biosensors procured from Cardea Bio (now Paragraf) involved a previously reported method.[11,14–16,29] In brief, Ti/Pt source, drain, and reference electrodes were patterned on 6-inch silicon wafers via lift-off technique and cleaned with piranha etching to remove organic residue contamination. Graphene film, grown on copper foil and supported by a spin-coated PMMA layer was delaminated using a bubbling method, was transferred onto the electrode-patterned wafers, and cleaned with acetone and isopropanol.[30] The graphene sheets were patterned to create defined channels between the source and drain electrodes. This was achieved through plasma-enhanced chemical vapor deposition, depositing a silicon oxide layer over the entire wafer, and subsequent reactive ion etching to etch the graphene transistors.[31] Two-terminal electrical resistance characterization of the devices demonstrated a yield of over 98% for functional graphene devices. The patterned graphene wafers were then diced into 9 mm × 9 mm die and each chip was connected to a custom-printed circuit board package using traditional wire bonding. The circuit board underwent encapsulation in epoxy, leaving an open cavity above the exposed graphene transistors for the placement of biological samples.

gFET functionalization

For glucose detection, chips were washed four times each using deionised (DI) H_2O, followed by 1X PBS (pH 7.4), and then one-time DMF. Fifteen microliter 10 mM PBA in DMF was added to the chips and incubated at room temperature (RT) for 45 min. Subsequently, the chips were rinsed two times with DMF, EtOH, one time IPA, and four times 1X PBS. PBA was activated by adding 100 mM EDC in 50 mM MES at pH 5.0 to the chips followed by a 30-min incubation at RT and removed excess EDC by four-time wash using 50 mM MES at pH 5.0. Then, 10 mg/mL GOX in 50 mM acetate buff at pH 4.0 was added and incubated for 2 h at RT on a shaker. After incubation, chips were washed four times with acetate buffer (50 mM, pH 4.0).

For pH sensing, gFET sensors were cleaned using DI water and DMF and dried sensors were further exposed to different pH buffers to monitor the pH changes in buffer and in cell culture media with and without 25 μM of alizarin.

For antibody detection, gFETs were functionalized using 10 mM of 1-PBASE prepared in DMF and incubated for 1 h at RT. The chip was rinsed two times each with DMF, EtOH, and IPA, 1X PBS buffer, respectively, to desorb excess PBASE molecules. PBASE-functionalized gFET chips were subsequently functionalized with protein A (50 μM) via peptide bond formation in 1X PBS (pH 7.4) by incubating for 30 min at RT. gFET chips were then rinsed three times with 1X PBS to desorb nonspecifically bound protein A. Any remaining unreacted *N*-hydroxysuccinimide ester groups were quenched with 20 mM of ethanolamine (Alfa Aesar) in 1X PBS by 10-min incubation at RT (Fig. 2).

Glucose monitoring

Real-time monitoring of gFET responses was performed using a commercial reader (CardeaBio now Paragraf Pvt. Ltd). For glucose sensing, GOX-gFETs were exposed to D-glucose to detect the GOX-mediated generation of H_2O_2. After rinsing the chips twice with 1X PBS, D-glucose was sequentially introduced at concentrations of 5, 10, 15, 20, 25, and 30 mM, and Dirac voltage was monitored for 5 or 10 min with intermittent 1X PBS washing at RT (Supplementary Table S1). For control experiments, H_2O_2 was sequentially added to the chips at increasing concentrations of 25, 50, 75, 100, 125, and 150 μM, and measured Dirac shift for 5 min at RT. The chips were rinsed twice with 1X PBS at the end of D-glucose and H_2O_2 measurements. For glucose detection in cell culture media, bioreactor samples were diluted 1:3 in 1X PBS and spiked with D-glucose at concentrations of 0, 0.5, 1, 5, and 10 mM. To evaluate sensor specificity, different concentrations (0–10 mM) of L-glucose were exposed to GOX functionalized gFET. Sensor specificity was assessed by exposing the GOX-gFETs to L-glucose for 10 min at concentrations ranging from 0 to 10 mM. To further verify the glucose concentration, Cedex® Bio HT Analyzer was used to monitor glucose levels using equivalent concentrations as used for gFET-based detection.[9,32]

pH monitoring

pH response of bare gFET was performed using Tris-HCl buffer at different pH values. To prepare the buffer sample, 1M Tris-HCl was diluted to 200 mM using DI H_2O. The pH was confirmed with a pH probe and was adjusted to the desired values using HCl to pH 6.8, pH 7.6, and pH 8.2. Following this, the solution was diluted to a final concentration of 20 mM. The pH at this concentration was verified using a Fisher Scientific Education pH meter and the samples were aliquoted for further study. Before the addition of the sample to the chips, alizarin stock (10 mM) in DMF was added to each sample to get a final concentration of 25 μM. To perform the pH analysis in cell culture media, a 2.5% v/v cell culture media was mixed with Tris-HCl buffer (20 mM) of respective pH. The pH of the media was confirmed with a pH probe. For real-time monitoring of pH, bare graphene chips were washed four times with DI water followed by four washes with 1X PBS. Following this step, three calibration steps were performed, each with 1X PBS and a 5-min incubation. Then, the 30 μL test sample was added to the chips in two quick successions, with the second addition undergoing a 30-min incubation step (Supplementary Table S2).

The Bigger Picture

This study highlights the potential of real-time monitoring of products and byproducts through advanced graphene-based sensors, enabling biomanufacturing processes to become more autonomous. By continuously tracking critical parameters, this technology can enhance production efficiency, optimize quality, and reduce waste, driving the future of biomanufacturing toward greater precision and self-regulation.

Antibody detection

For IgG detection, protein A immobilized chips calibration was performed by 5 min measurement of 1X PBS two times. Next, IgG1 was added with sequentially increasing concentrations: 0, 25, 50, 100, and 200 μg/mL, allowing a 30-min incubation for each addition. Two washes with 1X PBS were performed between each addition, followed by a calibration step with 1X PBS by 5-min incubation (Supplementary Table S3). CHO cell filtrate was measured by doping 0, 0.1, and 0.5% v/v in 1X PBS.

Data analysis

For each experiment, data from at least three chips were collected for every condition tested. Chips were exposed to various concentrations of analytes to assess the response range of the gFETs. The distribution was analyzed using the Shapiro–Wilk test for the control and test samples. Subsequently, a parametric *t*-test with Welch correction was conducted with normally distributed control and test samples. The mean data and standard deviation were plotted using GraphPad Prism 10.

Acknowledgments

The authors are thankful to Agilent for their generous support of the Aran lab. The authors also thank Kristin Bernick for her role in facilitating the grant and discussing the results. The authors are grateful to the Amgen Bioprocess lab at Keck Graduate Institute for providing cell culture samples and access to their bioprocessing facilities.

Authors' Contributions

All the experiments presented in the article were performed under the supervision of K.A. The glucose sensing experiment and data analysis performed by M.C., R.H., and D.K.B. R.H. introduced the alizarin reporter for pH sensing. pH with Tris-HCl buffer and antibody sensing experiment reported in the article designed by D.K.B., R.H. and performed by M.C. with D.K.B. S.A., and S.D. provided CHO cell bioprocess samples and help biolayer interferometry experiment. All the biolayer interferometry

experiments presented in the article were performed and analyzed by M.C. with D.K.B. D.K.B., M.C., F.B., and K.A. participated in article writing. All the authors have provided feedback for the article and consent to publish the work.

Author Disclosure Statement

No competing financial interests exist.

Funding Information

This work was further supported by the NSF (Grant No. 2048283) and the NIH (Grant No. 1R01HL16136) and gift support from Agilent to Aran lab.

Supplementary Material

Supplementary Figure S1
Supplementary Figure S2
Supplementary Figure S3
Supplementary Figure S4
Supplementary Table S1
Supplementary Table S2
Supplementary Table S3

References

1. Rathore AS, Mishra S, Nikita S, et al. Bioprocess control: Current progress and future perspectives. Life (Basel) 2021;11(6); doi: 10.3390/life11060557
2. Clementschitsch F, Bayer K. Improvement of bioprocess monitoring: Development of novel concepts. Microb Cell Fact 2006;5(1):19; doi: 10.1186/1475-2859-5-19
3. Reardon KF. Practical monitoring technologies for cells and substrates in biomanufacturing. Curr Opin Biotechnol 2021;71:225–230; doi: 10.1016/j.copbio.2021.08.006
4. Liu B, Villacres-Barragan C, Lattova E, et al. Differential affects of low glucose on the macroheterogeneity and microheterogeneity of glycosylation in CHO-EG2 camelid monoclonal antibodies. BMC Proc 2013;7(S6):P112; doi: 10.1186/1753-6561-7-S6-P112
5. Li F, Vijayasankaran N, Shen A, et al. Cell culture processes for monoclonal antibody production. MAbs 2010;2(5):466–479; doi: 10.4161/mabs.2.5.12720
6. Kim HS, Lee GM. Differences in optimal ph and temperature for cell growth and antibody production between two chinese hamster ovary clones derived from the same parental clone. J Microbiol Biotechnol 2007;17(5):712–720.
7. Ahleboot Z, Khorshidtalab M, Motahari P, et al. Designing a strategy for pH control to improve CHO cell productivity in bioreactor. Avicenna J Med Biotechnol 2021;13(3):123–130.
8. Tran T, Eskilson O, Mayer F, et al. Real-time nanoplasmonic sensor for IgG monitoring in bioproduction. Processes 2020;8(10):1302; doi: 10.3390/pr8101302
9. Lederle M, Tric M, Roth T, et al. Continuous optical in-line glucose monitoring and control in CHO cultures contributes to enhanced metabolic efficiency while maintaining darbepoetin alfa product quality. Biotechnol J 2021;16(8):e2100088; doi: 10.1002/biot.202100088
10. Suvarnaphaet P, Pechprasarn S. Graphene-Based materials for biosensors: A review. Sensors (Basel) 2017;17(10); doi: 10.3390/s17102161
11. Goldsmith BR, Locascio L, Gao Y, et al. Digital biosensing by foundry-fabricated graphene sensors. Sci Rep 2019;9(1):434; doi: 10.1038/s41598-019-38700-w
12. Ban DK, Bandaru PR. Graphene and two-dimensional materials for biomolecule sensing. Annu Rev Biophys 2023;52:487–507.
13. Peña-Bahamonde J, Nguyen HN, Fanourakis SK, et al. Recent advances in graphene-based biosensor technology with applications in life sciences. J Nanobiotechnology 2018;16(1):75; doi: 10.1186/s12951-018-0400-z
14. Hajian R, Balderston S, Tran T, et al. Detection of unamplified target genes via CRISPR–Cas9 immobilized on a graphene field-effect transistor. Nat Biomed Eng 2019;3(6):427–437; doi: 10.1038/s41551-019-0371-x
15. Balderston S, Taulbee JJ, Celaya E, et al. Discrimination of single-point mutations in unamplified genomic DNA via Cas9 immobilized on a graphene field-effect transistor. Nat Biomed Eng 2021;5(7):713–725; doi: 10.1038/s41551-021-00706-z
16. Ban DK, Hajian R, Winton AJ, et al. A single multiomics transistor for electronic detection of SARS-Cov2 variants antigen and viral RNA without amplification. Adv Materials Technologies 2023;8(11):2201945; doi: 10.1002/admt.202201945
17. Bauer JA, Zámocká M, Majtán J, et al. Glucose oxidase, an enzyme "Ferrari": Its structure, function, production and properties in the light of various industrial and biotechnological applications. Biomolecules 2022;12(3); doi: 10.3390/biom12030472
18. Vogt S, Schneider M, Schäfer-Eberwein H, et al. Determination of the pH dependent redox potential of glucose oxidase by spectroelectrochemistry. Anal Chem 2014;86(15):7530–7535; doi: 10.1021/ac501289x
19. Weibel MK, Bright HJ. The glucose oxidase mechanism: Interpretation of the pH dependence. J Biol Chem 1971;246(9):2734–2744; doi: 10.1016/S0021-9258(18)62246-X
20. Rogers M, Brandt K. Interaction of halide ions with Aspergillus niger glucose oxidase. Biochemistry 1971;10(25):4630–4635.
21. Salvo P, Melai B, Calisi N, et al. Graphene-based devices for measuring pH. Sens Actuators B Chem 2018;256:976–991; doi: 10.1016/j.snb.2017.10.037
22. Hao Z, Zhu Y, Wang X, et al. Real-time monitoring of insulin using a graphene field-effect transistor aptameric nanosensor. ACS Appl Mater Interfaces 2017;9(33):27504–27511; doi: 10.1021/acsami.7b07684
23. Zhou H-X, Pang X. Electrostatic interactions in protein structure, folding, binding, and condensation. Chem Rev 2018;118(4):1691–1741; doi: 10.1021/acs.chemrev.7b00305
24. Turcanu A, Bechtold T. pH dependent redox behaviour of alizarin Red S (1,2-dihydroxy-9,10-anthraquinone-3-sulfonate) – Cyclic voltammetry in presence of dispersed vat dye. Dyes Pigments 2011;91(3):324–331; doi: 10.1016/j.dyepig.2011.04.011
25. Jassam N, Jones CM, Briscoe T, et al. The hook effect: A need for constant vigilance. Ann Clin Biochem 2006;43(Pt 4):314–317; doi: 10.1258/000456306777695726
26. Priyadarshini S, Manas F, Prabhu S. False negative urine pregnancy test: Hook effect revealed. Cureus 2022;14(3):e22779.
27. Gargalo CL, Udugama I, Pontius K, et al. Towards smart biomanufacturing: A perspective on recent developments in industrial measurement and monitoring technologies for bio-based production processes. J Ind Microbiol Biotechnol 2020;47(11):947–964; doi: 10.1007/s10295-020-02308-1
28. Brookwell A, Oza JP, Caschera F. Biotechnology applications of cell-free expression systems. Life (Basel) 2021;11(12); doi: 10.3390/life11121367
29. Hajian R, DeCastro J, Parkinson J, et al. Rapid and electronic identification and quantification of age-specific circulating exosomes via biologically activated graphene transistors. Adv Biol 2021;5(7):2000594; doi: 10.1002/adbi.202000594
30. Gao L, Ren W, Xu H, et al. Repeated growth and bubbling transfer of graphene with millimetre-size single-crystal grains using platinum. Nat Commun 2012;3(1):699; doi: 10.1038/ncomms1702
31. Stine R, Mulvaney SP, Robinson JT, et al. Fabrication, optimization, and use of graphene field effect sensors. Anal Chem 2013;85(2):509–521; doi: 10.1021/ac303190w
32. Hofer A, Kroll P, Herwig C. Glucose monitoring and control using Numera®. Lucullus® PIMS and Cedex® Bio HT Analyzer 2018.

Received: August 31, 2024
Accepted: November 14, 2024
Online Publication Date: December 6, 2024